Boson Journal of Modern Physics (BJMP)
ISSN: 2454-8413

SCITECH
RESEARCH ORGANISATION

Volume 1, Issue 1
October12, 2015

Boson Journal of Modern Physics
www.scitecresearch.com

EPR, Optical Absorption and Superposition Model Studies of Cr3+ Doped Cesium Tetrabromozincate

Ram Kripal, Awadhesh Kumar Yadav
EPR Laboratory, Department of Physics, University of Allahabad, Allahabad-211002, India.

Abstract

Electron paramagnetic resonance (EPR) study of Cr^{3+} doped cesium tetrabromozincate (CTBZ) single crystal is done at room temperature. The hyperfine structure for Cr^{53} isotope is also obtained. Two magnetically inequivalent sites for Cr^{3+} are observed. The spin Hamiltonian parameters are evaluated as: D = 234×10^{-4}cm^{-1}, E = 69×10^{-4}cm-^{1}, g = 2.0104, A = 80×10^{-4} cm^{-1} for site I and D = 235×10^{-4} cm^{-1}, E = 70×10^{-4}cm^{-1}, g = 2.0061, A = 82×10^{-4}cm^{-1} for site II, respectively. The optical absorption spectra are recorded at room temperature. The energy values of different orbital levels are determined. The values of various parameters obtained are: B = 602 cm^{-1}, C = 2504 cm^{-1}, Dq = 1870 cm^{-1}, h = 1.63 and k = 0.21, where B and C are Racah parameters, Dq is crystal field parameter, and h and k are nephelauxetic parameters, respectively. Theoretical zero-field splitting (ZFS) parameters for Cr^{3+} at two sites in CTBZ are evaluated using superposition model and microscopic spin Hamiltonian theory. The theoretical ZFS parameters are in good agreement with the experimental values.

Keywords: A. Inorganic compounds; B. Crystal Growth; D. Crystal Fields; D. Electron Paramagnetic Resonance; D. Optical Properties.

PACS No: 76.30.Da; 76.30.Fc; 71.70.Ch.

1. Introduction

Electron paramagnetic resonance (EPR) study of transition metal ion doped single crystals is used to find the local site symmetry and zero-field splitting parameters [1]. The optical study is used to obtain crystal field strength and the energy level structure of the impurity ion. Cr^{3+} is one of the most investigated transition metal ions used as a probe for studying the structure and local symmetry of the crystal field in new materials [2–4]. Chromium is used as tanning agent in leather industry [5].

The theoretical studies on the spin Hamiltonian parameters of 3d ions in crystals suggested various mechanisms to contribute to ground state splitting of magnetic ion. The mostly used perturbation procedure treats cubic field and diagonal parts of free ion Hamiltonian as unperturbed Hamiltonian, whereas the spin-orbit coupling, the low-symmetry field, and off-diagonal part of free ion Hamiltonian are considered as perturbation [6].

Cesium tetrabromozincate, Cs_2ZnBr_4 (CTBZ) can show thermo sensitive photo-selective phenomenon like ammonium tetrabromozincate [7]. This developed our interest in CTBZ. In the present investigation, EPR and optical studies of Cr^{3+} ion in CTBZ single crystal are done to obtain information about the crystal field strength, energy level structure and the local site symmetry of the doped ion. The study is further used to describe the nature of bonding in the complex. Furthermore, zero-field splitting (ZFS) parameters are determined theoretically using superposition model (SPM) and microscopic spin Hamiltonian theory. The theoretical ZFS parameter values are in good agreement with the experimental ones.

2. Crystal Structure

The crystal structure of CTBZ is orthorhombic with space group *Pnma* having the unit cell dimensions a = 10.196 Å, b = 7.770 Å, c = 13.517 Å. The number of atoms per unit cell is four i.e. Z = 4 [8]. The bromine atoms Br (1), Br (2), Br (3) and Br (4) are located at the distances of 7.518 Å, 3.634 Å, 6.974 Å and 6.974 Å from Cs^+ ion in the host lattice.

3. Experimental

CTBZ single crystals were grown at room temperature by slow evaporation of an aqueous solution of cesium bromide and zinc bromide to which 0.1 wt% of $CrCl_3.6H_2O$ was added. The crystals grew in about 15-20 days. EPR spectra of Cr^{3+} doped CTBZ were recorded at room temperature on Varian X-Band E-112 (9.52 GHz) reflection type EPR spectrometer about the three mutually perpendicular crystallographic axes **a**, **b** and **c** at an interval of 10^o each using a goniometer. The optical spectra of the crystal were recorded on Unicam-5625 spectrophotometer in UV–Vis–NIR (195–1100 nm) region at room temperature.

4. Results and Discussion

The recorded EPR spectrum of Cr^{3+} doped CTBZ single crystal at room temperature, when the external magnetic field is along the **c**-axis, is shown in Fig.1 (a). EPR spectra consist of 24 lines with hyperfine structure. These lines in all three planes show the presence of two magnetically inequivalent sites of Cr^{3+} ions. The hyperfine structure shows the presence of a stable isotope of chromium (Cr^{53}) of about 9.55% abundance with electronic spin S = 3/2 and nuclear spin I = 3/2 [9]. The EPR spectrum is simulated using EasySpin [10] and the spin Hamiltonian parameters obtained as discussed later. The simulated EPR spectrum is shown in Fig. 1 (b).

EPR spectra of Cr^{3+} ion are analyzed using a spin Hamiltonian [9]:

$$\mathcal{H} = \mu_B B.g.S + D\left[S_Z^2 - \frac{1}{3}S(S+1)\right] + E(S_X^2 - S_Y^2) + AIS \qquad (1)$$

where the first, second, third and fourth terms represent the electron Zeeman interaction, axial zero-field splitting, rhombic zero-field splitting and hyperfine interaction, respectively. For a Cr^{3+} (d^3) ion, the zero-field splitting arises from the interaction of the S = 3/2 system with the non-cubic components of the ligand field .

The theoretical field positions of EPR transitions are obtained by using the equations of Ref. [11]. The calculated field positions of fine structure lines corresponding to different transitions for rotation in three mutually perpendicular planes are fitted to experimental values. The calculated (solid line) and experimental field positions (points) shown in Fig 2((a): site I; (b): site II) are in good agreement. The direction of the maximum overall splitting of EPR spectra is taken as the z-axis and that of the minimum as the x-axis [12]. The (x, y, z) system is parallel to the crystallographic **a**-, **b**-, **c**-axes. The Z-axis of symmetry adopted axes (SAA) is coincident with the crystal **c**-axis and the other two axes (X, Y) lie in the ab plane for site I, whereas the Z-axis of SAA is coincident with the crystal **b**-axis and the other two axes (X, Y) lie in the ac plane for site II. This indicates that the local site symmetry is approximately orthorhombic type I (D_{2h}) [13]. The SAA system (X, Y, Z) of Cr^{3+} doped CTBZ single crystal for both sites is shown in Fig. 3. g-values and their direction cosines with respect to crystallographic axes are obtained using diagonalization procedure [14]. The best fit spin Hamiltonian parameters g, D, E and A are given in Table 1. The experimentally obtained direction cosines of g for Cr^{3+} ion (Table 1) are compared with the direction cosines of different bonds obtained from crystal structure data [8] shown in Table 2. The direction cosines of Cs–Br (1) and Cs–Br (3) bonds agree reasonably well with the experimental direction cosines of g of Cr^{3+} ions. This indicates that Cr^{3+} substitutes at Cs^+ sites. Also the ionic radius of Cr^{3+} (0.63A˚) is less than the ionic radius of Cs^+ (1.74A˚). Thus, the Cr^{3+} ion can fit well at the place of Cs^+. This supports the conclusion drawn on the basis of direction cosines. The charge compensation takes place by forming vacancies at some cation sites. The impurity ion enters the CTBZ lattice in a similar manner as observed in other Cr^{3+} doped crystal [15].

5. Optical Absorption Analysis

The electronic configuration of Cr^{3+} ion gives rise to the free ion terms ^4F, ^4P, ^2G and several other doublet states out of which ^4F is the ground state. In octahedral surroundings, the strong field configuration $(t_{2g})^3$ yields the states $^4A_{2g}$, ^2E_g, $^2T_{1g}$ and $^2T_{2g}$. Out of these, the $^4A_{2g}$ state lies lowest and is the ground state for Cr^{3+} ion. The first excited state configuration $(t_{2g})^2(e_g)^1$ provides quartet states $^4T_{1g}(F)$ and $^4T_{2g}(F)$ and a number of doublet states , and in weak field ^4F state splits as $^4A_{2g}(F)$, $^4T_{2g}(F)$ and $^4T_{1g}(F)$ whereas ^4P as $^4T_{1g}(P)$. In the doublet states, ^2G splits as $^2A_{1g}(G)$, $^2E_g(G)$, $^2T_{1g}(G)$ and $^2T_{2g}(G)$ and ^2H as $^2E_g(H)$, $^2T_{1g}(H)$ and $^2T_{2g}(H)$. The weak field terms $^4A_{2g}(F)$, $^2E_g(G)$, $^2T_{1g}(G)$ and $^2T_{2g}(G)$ correspond to the lowest strong field configuration t_{2g}^3. However, the ground state is $^4A_{2g}(F)$ at all strengths of the crystal field. Thus, only two spin

allowed transitions are obtained from $^4A_{2g}(F) \rightarrow {}^4T_{2g}(F)$ and $^4A_{2g}(F) \rightarrow {}^4T_{1g}(F)$ states in addition to several spin forbidden transitions. If the symmetry is lowered, the degeneracy will be lifted and several absorption bands observed. The optical spectra of Cr^{3+} doped CTBZ recorded at room temperature are shown in Fig.4 (a, b). These exhibit two intense bands located at 18691 and 25000 cm^{-1} and nine weak bands located at 11049, 12048, 13793, 15503, 17897, 20408, 31746, 40816 and 47619cm^{-1}, respectively. The two intense bands observed at 18,690 and 25,000 cm^{-1} correspond to the transitions $^4A_{2g}(F) \rightarrow {}^4T_{2g}(F)$ and $^4A_{2g}(F) \rightarrow {}^4T_{1g}(F)$, respectively. The three weak bands observed at 12,048, 15,503, 31,746 cm^{-1} are assigned to the spin forbidden transitions from $^4A_{2g}(F)$ to $^2E_g(G)$, $^2T_{1g}(G)$, $^2A_{1g}(G)$, respectively. The band at 11049 cm^{-1} is the component band of the transition $^4A_{2g}(F) \rightarrow {}^2E_g(G)$. The two weak bands observed at 40,816 and 47619 cm^{-1} are assigned to charge transfer (CT) bands [16]. Similarly, the band at 13793 cm^{-1} is the component band of the transition $^4A_{2g}(F) \rightarrow {}^2T_{1g}(G)$. The bands at 17897 and 20408 cm^{-1} are component bands of the transition $^4A_{2g}(F) \rightarrow {}^4T_{2g}(F)$.

The value of the crystal field parameter Dq and Racah parameter B are evaluated from the observed energy bands [17, 18]. The intense band position ν_1 at 18,691 cm^{-1} corresponding to the transition $^4A_{2g}(F) \rightarrow {}^4T_{2g}(F)$ gives the value 10Dq. The band at 25,000 cm^{-1} corresponding to $^4A_{2g}(F) \rightarrow {}^4T_{1g}(F)$ transition gives ν_2 and the Racah parameter B is given by the equation [19],

$$B = \left(2\nu_1^2 + \nu_2^2 - 3\nu_1\nu_2\right)/\left(15\nu_2 - 27\nu_2\right) \tag{2}$$

The value of B is evaluated as 602 cm^{-1}, which is significantly smaller than the free ion value of Cr^{3+}, B_{free} = 918 cm^{-1} [20, 21]. This decrease in B from B_{free} is caused by the effect of bond covalency. The Racah parameter C can be calculated from the position of the $^4A_{2g}(F) \rightarrow {}^2E_g(G)$ transition using the following equation [22],

$$\frac{C}{B} = \frac{1}{3.05}\left[\left(\frac{E(^2E)}{B}\right) - 7.9 + 1.8\left(\frac{B}{Dq}\right)\right] \tag{3}$$

The energy matrices [17, 18] for d^3 configuration in octahedral symmetry have been diagonalised for different values of B, C and Dq. The best fit of the observed bands is obtained for Dq = 1870, B = 602 and C = 2504 cm^{-1}.

The calculated and experimental band positions are in good agreement for Dq = 1870 cm^{-1} as shown in Fig 5**.** The band positions and their assignments are given in Table 3. The bonding in Cr^{3+}: CTBZ can be predicted by nephelauxetic parameters h and k of ligands and the central metal ion, respectively. h is obtained from the expression [23],

$$h = \left|(B_{free} - B)/B_{free}\right|/k_{Cr^{3+}} \tag{4}$$

which is 1.63, since the value of k for Cr^{3+} is 0.21 [24]. The larger value of h gives delocalization of the d electrons suggesting the predominantly ionic nature of bonding between Cr^{3+} and ligands. By correlating optical and EPR data, the chemical bonding parameter α' is obtained by [25],

$$g = g_e - 8\alpha'\lambda/\Delta \tag{5}$$

$$\lambda_{eff} = \alpha'\lambda$$

where g_e is the g-value of free electron (2.0023), λ is the spin–orbit coupling constant (91 cm^{-1}) [17], Δ is the gap between the excited and ground levels, λ_{eff} is the spin–orbit coupling constant for ion (Cr^{3+}) in the crystal [8]. From the experimental values g = 2.0104 and Δ = 18690 cm^{-1} for site I and g = 2.0061 and Δ = 18690 cm^{-1} for site II, the values of α' are 0.21 for site I and 0.10 for site II.

The value $0 < \alpha' < 1$ is characterized by the ionic contribution of the chemical bond between the Cr^{3+} ion and its ligands. Thus, the evaluated value of α' suggests the ionic nature of Cr^{3+} ion in CTBZ. The value of λ_{eff} is evaluated as 19 cm^{-1}(site I) and 9 cm^{-1}(site II). Its deviation from the free ion value can be attributed to bonding effects in the crystal which yield a reduction in the effective value of spin–orbit coupling and also in orbital moment. The value of Dq/B obtained (3.1) is of the order of Dq/B = 2.8 found for Al_2O_3: Cr^{3+} [26], which shows that the Cr^{3+} ions in CTBZ are situated in a strong crystal field. The ^2E_g state is unsplit in undistorted octahedral symmetry of the Cr^{3+} site [27]. But it splits in trigonal, tetragonal or orthorhombic distortions (low-symmetry fields) [21].

In the present study since the band associated with ^2E_g shows splitting, the distortion can be of any of the above three types. The T_{1g} or T_{2g} level splits into two components each in tetragonal and three components each in orthorhombic distortion. Since the band associated with T_{2g} level here splits into three components, the distortion is expected to be of orthorhombic type [21]. The values of Dq, B and C are in the range reported for $Cr(NH_3)_6^+$ [28]. We would expect the crystal field strength to be larger in CTBZ as in MgO [9] and therefore a Dq value as in $Cr(NH_3)_6^+$ or even larger can be expected.

The spin-orbit splitting can be evaluated from the relation of Cole and Garret [29],

$$\lambda_{eff} = 0.0011(B+1.08)3+0.0062 \tag{6}$$

where the Racah parameter B and spin–orbit coupling constant λ_{eff} are in kK. The value of λ_{eff}, thus determined from the above expression is 79 cm^{-1}. This value is in good agreement with the value expected for the Cr^{3+} ion in crystals having oxygen ligands, like in MgO [28]. It is interesting to compare this value with the value obtained from EPR and optical studies.

6. Theoretical Investigation

The energy level of the ground state of transition metal ion doped in crystal can be described using the spin Hamiltonian consisting of Zeeman electronic (Ze) and ZFS terms [30]. Explicit form of the ZFS terms for Cr^{3+} ion with S = 3/2 at orthorhombic symmetry site (D_{2h}) can be written as:

$$\begin{aligned} \mathcal{H} &= B_2^0 O_2^0 + B_2^2 O_2^2 + AIS = \frac{1}{3} b_2^0 O_2^0 + \frac{1}{3} b_2^2 O_2^2 + AIS \\ &= D(S_z^2 - \frac{1}{3} S(S+1)) + E(S_x^2 - S_y^2) + AIS \end{aligned} \tag{7}$$

The ZFSPs in Eq. (7) can be obtained using SPM. Conventional zero field splitting parameters were derived [31-34] for $3d^3$ ion at orthorhombic symmetry as

$$\mathrm{D} = b_2^0 = \frac{\bar{b}_2(R_0)}{2}\left[\left(\frac{R_0}{R_i}\right)^{t_2} \sum_i (3\cos^2\theta_i - 1)\right] \tag{8}$$

$$\mathrm{E} = \frac{b_2^2}{3} = \frac{\bar{b}_2(R_0)}{2}\left[\left(\frac{R_0}{R_i}\right)^{t_2} \sum_i \sin^2\theta_i \cos 2\phi_i\right] \tag{9}$$

For Cr^{3+} ions, the parameters of the rank k = 2 and 4 exist for crystal field parameters (CFPs), while only of the rank k = 2 for ZFSPs.

In CTBZ single crystal, the local symmetry around Cr^{3+} ion is slightly lower than orthorhombic. However, the calculations are done under the approximation of orthorhombic symmetry. For octahedral co-ordination around Cr^{3+} ion in the crystal, the parameters t_2 and $\bar{b}_2(R_0)$ for Cr^{3+} ion in case of $LiNbO_3$ having Cr^{3+} -O^{2-} bond are: t_2 = 0.12 and $\bar{b}_2(R_0)$ = 2.34 cm^{-1} [35]. The above parameters are used in our case for Cr^{3+} -O^{2-} bond.

Cr^{3+} ion enters the lattice of CTBZ substitutionally at site I and site II. The position of metal ion and spherical coordinates of ligands are given in Table 4. The calculated and conventional ZFS parameters together with reference distance are shown in Table 5. For the evaluation of ZFSPs, the reference distances of 0.205 nm and 0.179 nm were fixed. The calculated conventional ZFSPs are: D = 240 ×10^{-4} cm^{-1}, E = 64×10^{-4} cm^{-1} and D = 230 ×10^{-4} cm^{-1}, E = 75×10^{-4} cm^{-1} for site I and site II, respectively. The ratio b_2^2/b_2^0 is within the range (0, 1) for orthorhombic symmetry [12]. Here, the ratio of b_2^2/b_2^0 = 0.800, E/D = 0.266 for site I and b_2^2/b_2^0 = 0.937, E/D = 0.326 for site II. The theoretical ZFS parameters are in reasonable agreement with the experimental ones. The other reference distance obtained for oxide ligands [30] was also used but the ZFSPs determined were found very different as compared to the experimental values.

The CFPs for Cr^{3+} in crystals are obtained by the SPM formula [36]:

$$B_{kq} = \sum_i \bar{B}_k \left(\frac{R_0}{R_i} \right)^{t_k} K_{kq}(\theta_i \phi_i) \qquad (11)$$

where R_0 is the reference distance for the site; R_i, θ_i, φ_i are the polar coordinates of the i^{th} ligand and K_{kq} is the coordination factor [37]. For calculating B_{kq} (k = 2, 4; q = 0, 2, 4), $\bar{B}_2$ = 40, 400 cm^{-1}, t_2 = 1.3, $\bar{B}_4$ = 11, 700 cm^{-1} and t_4 = 3.4 are taken from Ref. [37]. The calculated B_{kq} parameters are given in Table 6. These parameters are used to calculate optical absorption spectra with the help of CFA program [38-39]. The energy levels of the impurity ion are obtained by diagonalizing the complete Hamiltonian within the $3d^N$ basis of states in the intermediate crystal field coupling scheme. The Hamiltonian contains the Coulomb interaction (in terms of B and C), Trees correction, the spin-orbit interaction, the crystal field Hamiltonian, the spin-spin interaction and the spin-other-orbit interaction. The calculated energy values are given in Table 7 together with the experimental values for comparison. It is found that there is good agreement between the two values.

7. Conclusion

EPR and optical studies of Cr^{3+} doped CTBZ single crystal have been carried out at room temperature .The spin Hamiltonian parameters (D, E, g and A) have been evaluated. The Cr^{3+} ions enter the lattice substitutionally by replacing Cs^+ ions .On the basis of EPR and optical data, the nature of bonding in the crystal has also been discussed. The values of the bonding parameters both from optical and EPR studies suggest that the bonding between Cr^{3+} and ligands is ionic. The hyperfine structure has been observed due to interaction of unpaired electron spin and nuclear spin.

Acknowledgement

The authors are thankful to the Head, SAIF, I.I.T. Mumbai, Powai, Mumbai for providing the facility of EPR spectrometer. One of the authors, Awadhesh Kumar Yadav is thankful to the Head, Department of Physics, University of Allahabad, Allahabad for providing departmental facilities.

References

[1] W. C. Zheng, S. Y. Wu, D. Hui-Ning, Z. Jian, Spectrochem. Acta A 58(2002)537-541.

[2] M. Casalboni, V. Ciafardone, G. Giuli, B. Izzi, E. Paris, .Prosposito, J. Phys.: Condens. Matter 8(1996)9059-9070.

[3] R. Jablonski, M. Palczewska, A. Pajaczkowska, J. Magn. Magn. Mater. 167(1997)99-104.

[4] M. G. Zhao, Y. Lei, J.Phys.: Condens. Matter 9 (1997)529-540.

[5] P. Sambasiva Rao, S. Subramanian, Mol. Phys. 39 (1980) 935-943.

[6] Z.Y. Yang, J. Phys.: Condens. Matter 12 (2000) 4091-4096.

[7] M. A. El-Sayed, Proc. SPIE 0620, Laser Applications in Chemistry and Biophysics, 126 (June 30,1986); oi:10.1117/12.961137.

[8] B. Morosin, E. C. Lingafelter, Acta Cryst. 12(1959) 744-745.

[9] A. Abragam, B. Bleaney, EPR of Transition Ions, Clarendon Press, Oxford, 1970.

[10] S. Stoll, A. Schweiger, J. Magn. Reson. 170(2006)42-55.

[11] F. B. I. Cook, M. J. A. Smith, J. Phys. C: Solid State Phys.7 (1974) 2353-2364.

[12] C. Rudowicz, R. Bramley, J. Chem. Phys. 83 (1985) 5192- 5197.

[13] C. Rudowicz, Y. Y. Zhao, W. L. Yu, J. Phys. Chem. Solids 53 (1992)1227-1236.

[14] D. S. Schonland, Proc. Phys. Soc. 73 (1958) 788-792

[15] W. C. Zheng, S. Y. Wu, Phys. Stat. Solidi B 207 (1998) 429-435.

[16] P. W. Atkins, T. L. Overton, J. P. Rourke, M. T. Weller, F. A. Armstrong, Inorganic Chemistry, 5th Ed., Oxford University Press, 2010.

[17] R. J. Peruma Reddy, Coordin. Chem. Rev. 4 (1969)73-105.

[18] Y. Tanabe, S. Sugano, J. Phys. Soc. Jpn. 9 (1954)753-766.

[19] F. Rasheed, K. P. O Donnel, B. McCollum, B. Henderson, D. B. Hollis, J. Phys: Condens. Matter 3 (1991) 1915-1930.

[20] C. E. Moore, Atomic Energy Levels, (Chromium through Niobium), National Bureau of Standard Circular No. 467, Vol. 2, US Government Printing Office, Washington, DC, 1948, 1952.

[21] R. V. S. S. N. Ravi Kumar, A. V. Chandrasekhar, S. N. Rao, N. Madhu, B. J. Reddy, Cryst. Res. Technol. 34 (1999) 911-914.

[22] K. T. Liu, J. T. Yu, S. H. Lou, C. H. Lee, Y. Huang, K. H. Li, J. Phys. Chem. Solids 55 (1994) 1221-1226.

[23] W. Seeber, D. Ehrt, D. Eberdorff-Heidepriem, J. Non-Cryst. Solids 171 (1994) 94-104.

[24] C. K. Jorgensen, Absorption Spectra and Chemical Bonding in Complexes, Plenum, Oxford, 62,p.113.

[25] M. Haouari, H. B. Ouada, H. Maaref, H. Hommel, A. P. Legrand, J. Phys.: Condens. Matter 9 (1997) 6711-6718.

[26] W. Ryba-Romanowski, S. Golab, W. A. Pisarski, D. Podsiadla, Z. Czapla, Chem. Phys. Lett. 264 (1997) 323-326.

[27] W. Ryba-Romanowski, S. Golab, G. Dominiak-Dzik, W. A.Pisarski, D. Podsiadla, Z. Czapla, J. Mol. Struct. 450 (1998) 219-222.

[28] B. N. Figgis, M. A. Hitchman, Ligand Field Theory and its Applications, Wiley- VCH, New York, 2000.

[29] G. M. Cole Jr., B. B. Garret, Inorg. Chem. 9 (1970)1898-1902.

[30] C. Rudowicz, C. Y. Chung, J. Phys.: Condens. Matter 16 (2004) 5825-5847; M. G. Brik, N. M. Avram (Eds.), Superposition Model and its applications in: Optical Properties of 3d-Ions in Crystals, Spectroscopy and Crystal Field Analysis, Springer, Heidelberg, 2013.

[31] M. Acikgoz, Spectrochim. Acta A 86(2012) 417-422.

[32] K. A. Muller, W. Berlinger, J. Phys. C: Solid State Phys. 16(1983) 6861-6874.

[33] M. Acikgoz, P. Gnutek, C. Rudowicz, Solid State Commun. 150(2010) 1077-1081.

[34] T. H. Yeom, Y. M. Chang, S. H. Choh, C. Rudowicz, Phys. Stat. Sol. b185 (1994), 409–41

[35] T. H. Yeom, Y. M. Chang, C. Rudowicz, Solid State Commun. 87(1993) 245-249.

[36] Y. Y. Yeung, C. Rudowicz, Y. M. Chang, J. Qin, J. Lumin. 60&61(1994) 108-111.

[37] Y. Y. Yeung, D. J. Newman, Phys. Rev. B 34(1986)2258-2265.

[38] Y. Y. Yeung, C. Rudowicz, Computers Chem. 16 (1992) 207-216.

[39] Y. Y. Yeung, C. Rudowicz, J. Comput. Phys. 109 (1993) 150-152.

Table and Figure Captions:

Table 1. Principal g values, their direction cosines and the parameters D, E and A.

Table 2. The ionic distances and direction cosines of different bonds of Cr^{3+} doped CTBZ single crystal.

Table 3. Observed and calculated energy bands and their assignments for Cr^{3+} doped CTBZ (Dq = 1870 cm^{-1}, B = 602 cm^{-1} and C = 2504 cm^{-1}).

Table 4. Fractional positions of Cr^{3+} ions together with spherical co-ordinates (R, θ, ø) of ligands in CTBZ single rystals.

Table 5. Calculated and conventional zero field splitting parameters together with

Reference distance for Cr^{3+} doped CTBZ single crystal.

Table 6. B_{kq} parameters to be used in CFA program for calculating optical absorption spectra.

Table 7.Observed and calculated energy bands and their assignments for Cr^{3+} doped CTBZ single crystal using CFA rogram.

Fig. 1. (a) EPR spectrum recorded in ab plane for magnetic field B at 0^0 from **c** axis.

(b) Simulated EPR spectrum in ab plane for magnetic field B at 0^0 from **c** axis (Frequency 9.11 GHz).

Fig. 2. Angular variation of EPR lines for Cr^{3+} doped CTBZ in all three planes for (a) Site I, (b) Site II.

Fig. 3. Crystal structure of CTBZ in which symmetry adopted axis system (SAAS) is shown.

Fig. 4 . Optical absorption spectrum of Cr^{3+} doped CTBZ recorded at room temperature in the wavelength range (a) 195-25 nm, (b) 325-1100 nm.

Fig. 5. Variation of energy levels of Cr^{3+} doped CTBZ with Dq for B = 602 cm^{-1}, C = 2504 cm^{-1} and α = 76 cm^{-1} (experimental energies are shown by circles).

Table 1

Site	Principal g values	**a**	**b**	**c**	D	E	A
I	g_x = 1.9831	-0.9900	0.0109	0.1403	234	69	80
	g_y = 2.0147	0.0242	0.9954	0.0930			
	g_z = 2.0336	**0.1387**	**-0.0955**	**0.9857**			
II	g_x = 1.9840	-0.9942	0.1007	- 0.0379	235	70	82
	g_y = 2.0128	0.1028	09931.	-0.0563			
	g_z = 2.0215	**-0.0320**	**0.0599**	**0.9977**			

D, E and A are in units of $10^{-4}cm^{-1}$ and estimated errors for g, D, E and A are ±0.0002 and $\pm 2\times10^{-4}cm^{-1}$ respectively.

Table 2

Bonds	Ionic Distances(Å)	Direction cosines with respect to crystallographic axes		
	R(Å)	**a**	**b**	**c**
$Cs\text{-}Br^{-}(1)$	6.4728	±0.6422	±0	±0.7664
$Cs\text{-}Br^{-}(2)$	4.2392	±0.4649	±0	±0.8853
$Cs\text{-}Br^{-}(3)$	3.7918	±0.2208	±0.2785	±0.9346
$Cs\text{-}Br^{-}(4)$	3.7918	±0.2208	±0.2785	±0.9346
$Cs\text{-}Br^{-}(5)$	3.7918	±0.8397	±0.5122.	±0.1800
$Cs\text{-}Br^{-}(6)$	4.2650	±0.3222	±0	±0.9466

Table 3

Transition from $^4A_{2g}(F)$	Observed wave number (cm^{-1})	Calculated wave number (cm^{-1})
$^2Eg(G)$	11049, **12048**	12200
$^2T_1g(G)$	13793,**15503**	14992
$^4T_2g(F)$	17897, **18691**, 20408	18700
$^4T_1g(F)$	25000	25642
$^2A_1g(G)$	31746	30490
$^2T_2g(H)$	40816	39648
$^2T_1g(H)$	47619	47826

Table 4

Position of Fe^{3+} (Fractional)	Ligands	Spherical co-ordinates of ligand		
		R(Å)	θ	ø
Site I : Substitutional	Br^-(1)	6.4728	90	0
(0,0,0)	Br^-(2)	4.2392	128	0
	Br^-(3)	3.7918	79	31
	Br^-(4)	3.7918	79	31
	Br^-(5)	3.7918	79	-31
	Br^-(6)	4.2650	18	0
Site II : Substitutional	Br^-(1)	6.8382	92	0
(0,0,0)	Br^-(2)	4.6435	94	0
	Br^-(3)	3.1746	83	33
	Br^-(4)	3.1746	83	33
	Br^-(5)	3.2820	81	30
	Br^-(6)	4.2910	24	0

Table 5

		Zero-field splitting parameters (cm^{-1})			Cnventional Zero-field splitting parameters ($\times 10^{-4} cm^{-1}$)		
	R_0(Å)	b_2^0	b_2^2	b_2^2 / b_2^0	D	E	E/D
Site I	2.05.	-0.0240	0.0192	0.800	240	64	0.266
Site II	1.79	-0.0230	0.0225	0.937	230	75	0.326

Table 6

	B_{kq} (cm^{-1}) Parameters used for CFA package					
	R_0(Å)	B_{20}	B_{22}	B_{40}	B_{42}	B_{44}
Site I	2.05	54103	18917	-24047	11723	-38461
Site II	1.79	56107	17915	-23049	10726	-39484

Table 7

Transition from $^4A_{2g}$(F)	Experimentally observed band (cm^{-1})	Calculated energy bands from CFA (cm^{-1})
^{2}Eg(G)	11049,**12048**	12342,12652
$^2T_1$g(G)	13793,**15503**	13731,14837,15362
$^4T_2$g(F)	17857,**18691**,20408	17586,17439,17785,18261,18285,18430
$^4T_1$g(F)	25000	24088,24120,24180,24315,24344,24420
$^2A_1$g(G	31746	31583
CT band	40816	40615
CT band	47619	47639

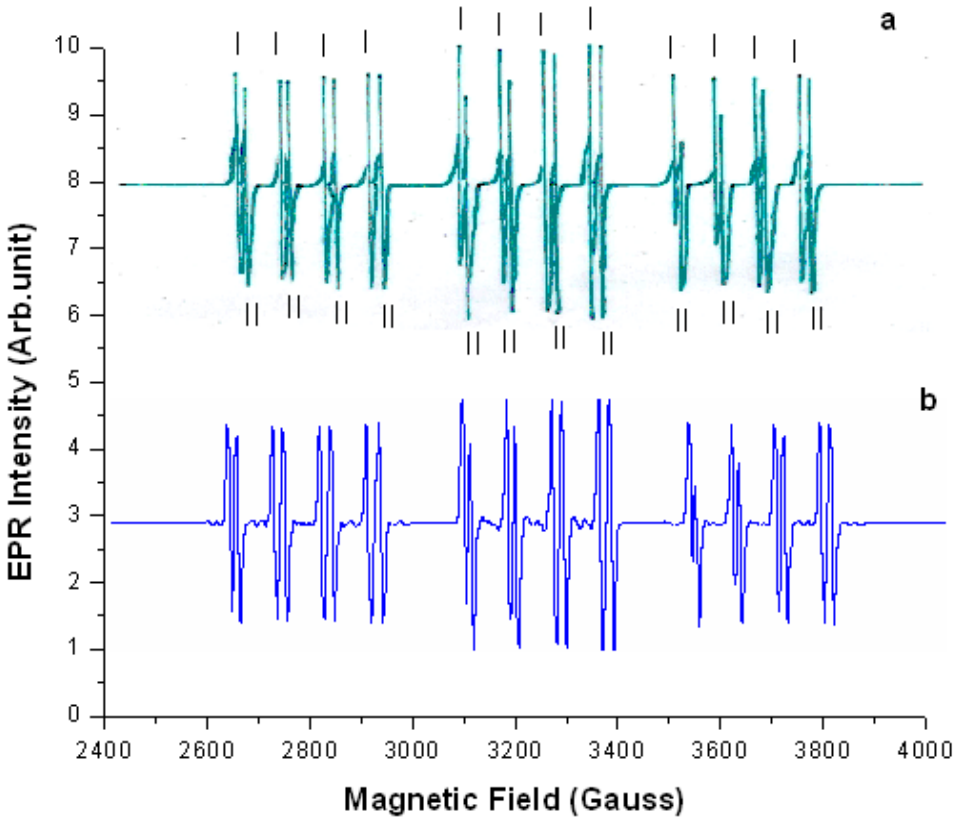
a
b
EPR Intensity (Arb.unit)
Magnetic Field (Gauss)
0
1
2
3
4
5
6
7
8
9
10
2400
2600
2800
3000
3200
3400
3600
3800
4000

Fig. 1

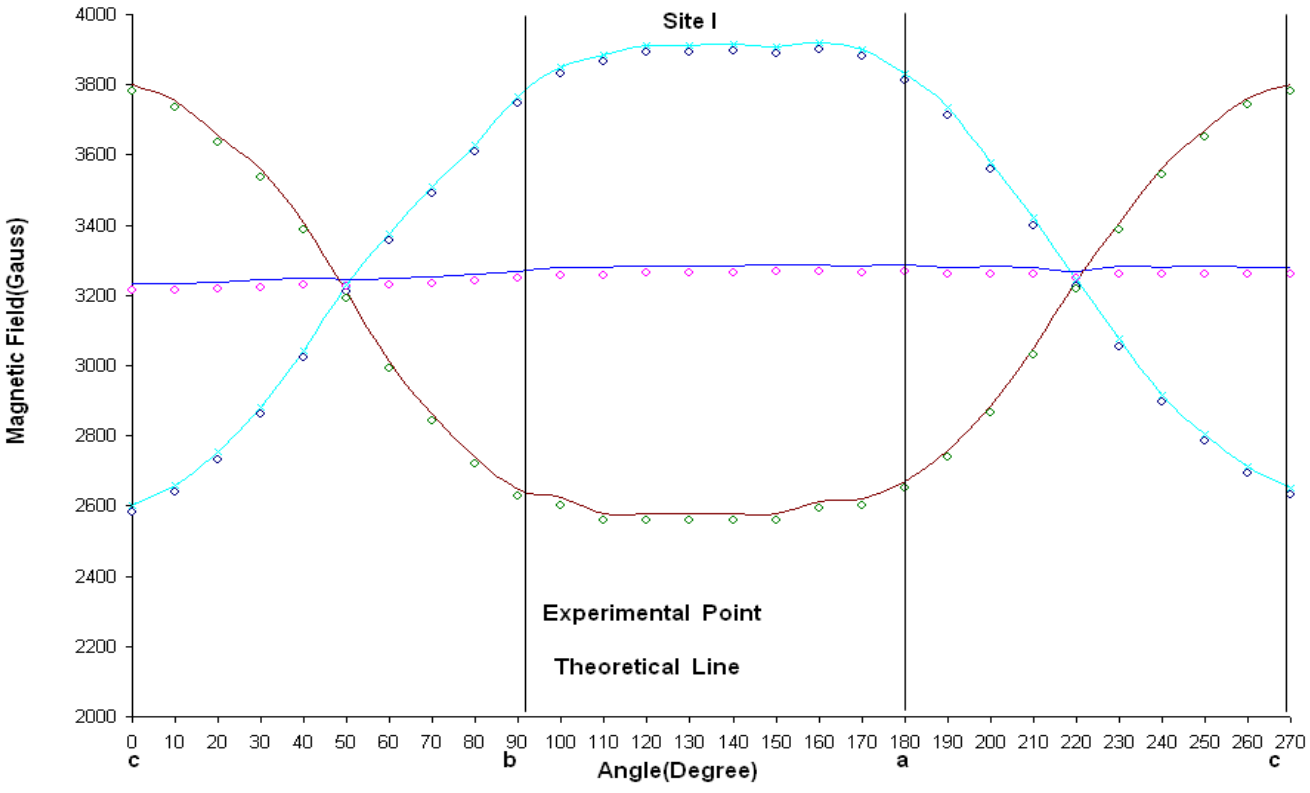
Site I
Experimental Point
Theoretical Line
Magnetic Field(Gauss)
Angle(Degree)
c
b
a
c
2000
2200
2400
2600
2800
3000
3200
3400
3600
3800
4000
0
10
20
30
40
50
60
70
80
90
100
110
120
130
140
150
160
170
180
190
200
210
220
230
240
250
260
270

Fig. 2 (a)

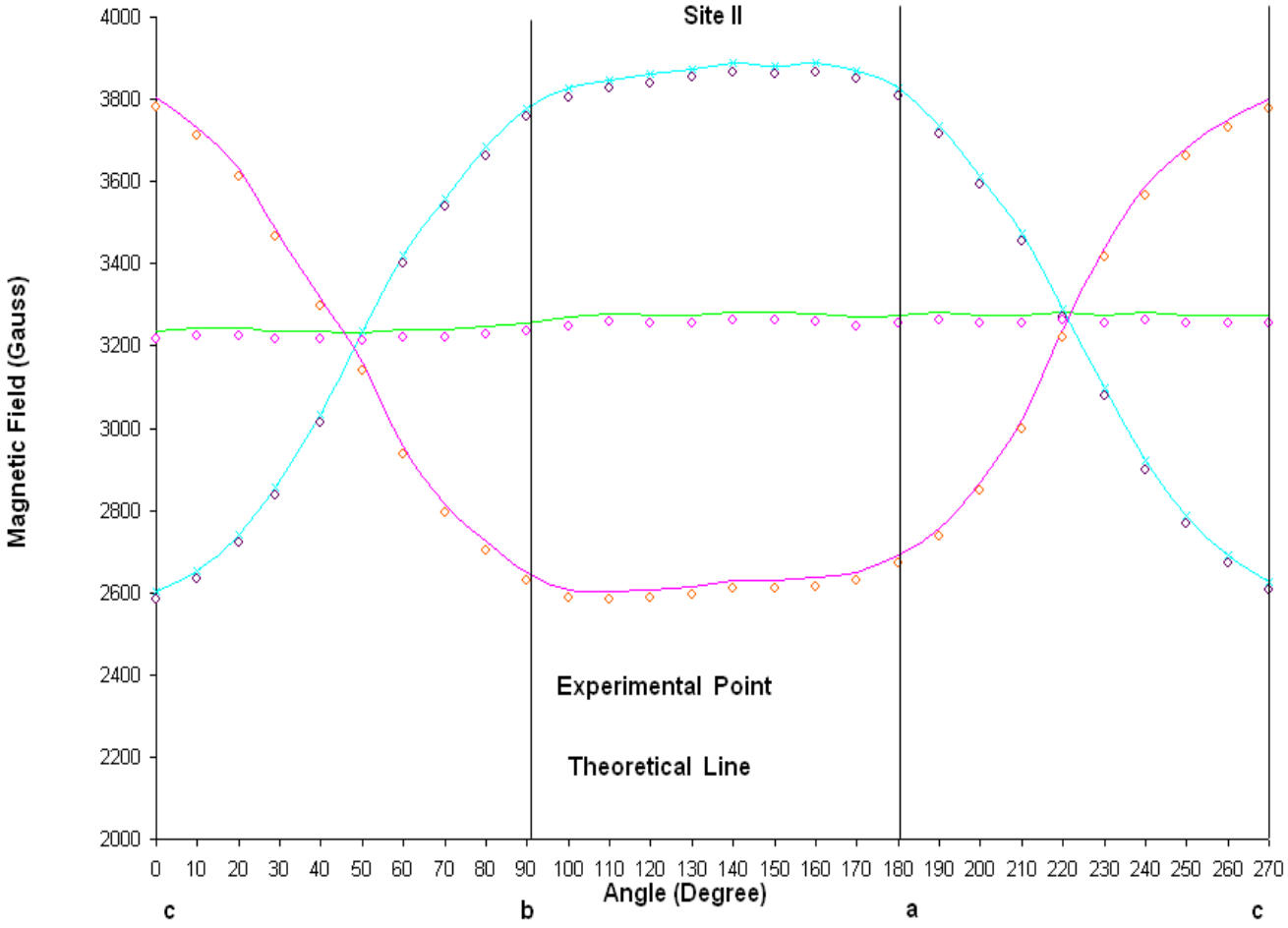
Site II
Magnetic Field (Gauss)
4000
3800
3600
3400
3200
3000
2800
2600
2400
2200
2000
Experimental Point
Theoretical Line
0 10 20 30 40 50 60 70 80 90 100 110 120 130 140 150 160 170 180 190 200 210 220 230 240 250 260 270
Angle (Degree)
c
b
a
c

Fig. 2(b)

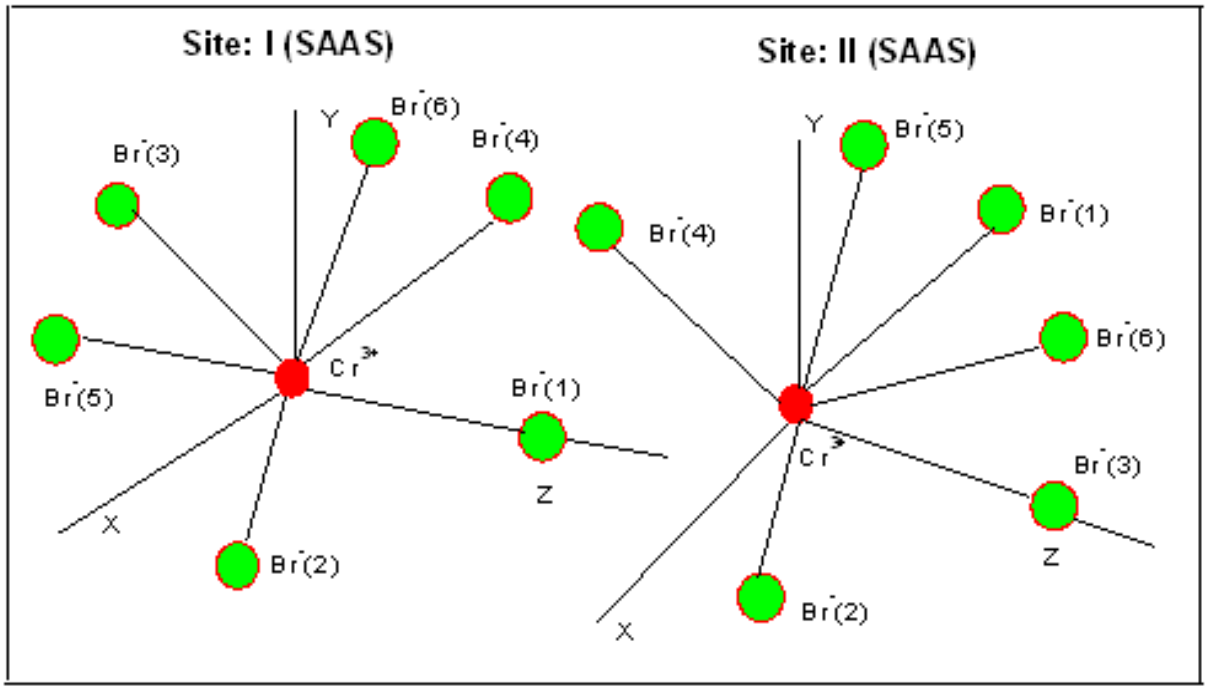
Site: I (SAAS)
Site: II (SAAS)
Br(3)
Y
Br(6)
Br(4)
Br(5)
Cr3+
Br(1)
Z
X
Br(2)
Y
Br(5)
Br(4)
Br(1)
Br(6)
Cr3+
Br(3)
Z
Br(2)
X

Fig. 3

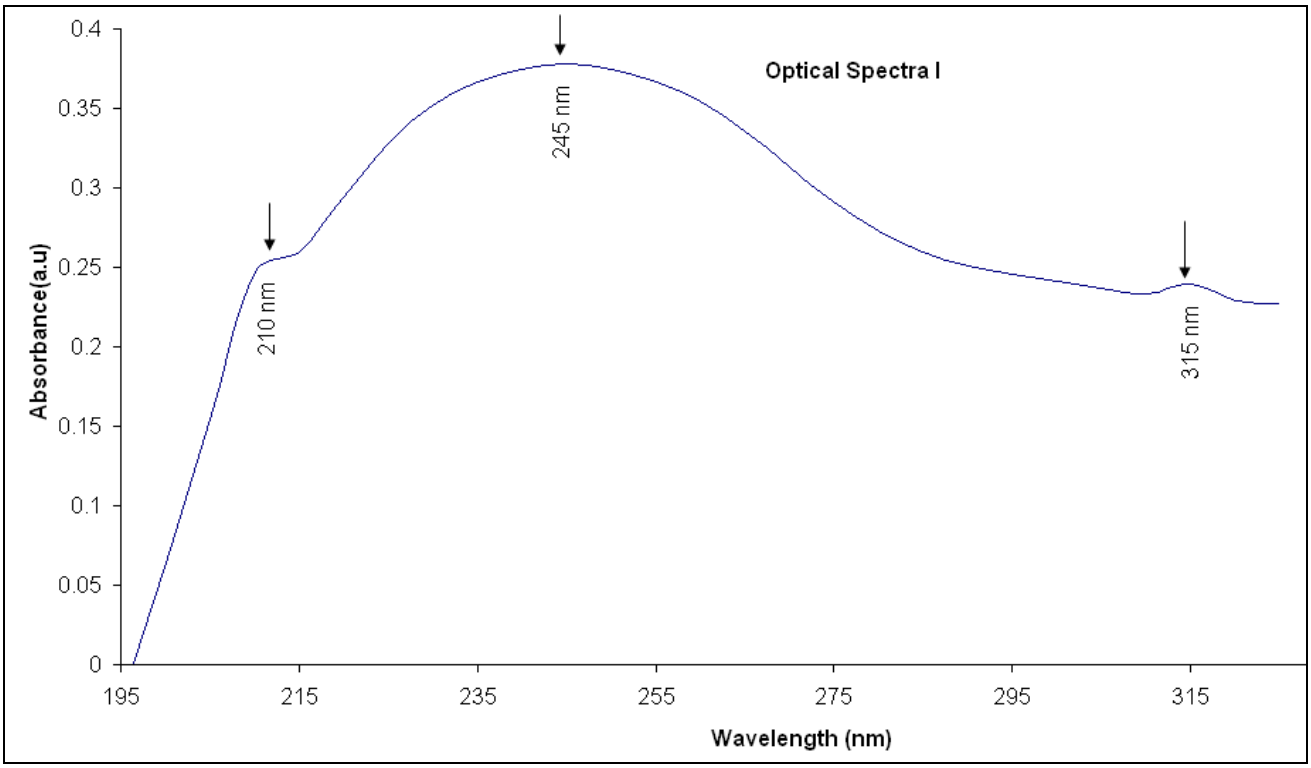
Optical Spectra I
Absorbance(a.u)
Wavelength (nm)
0.4
0.35
0.3
0.25
0.2
0.15
0.1
0.05
0
195
215
235
255
275
295
315
210 nm
245 nm
315 nm

Fig. 4(a)

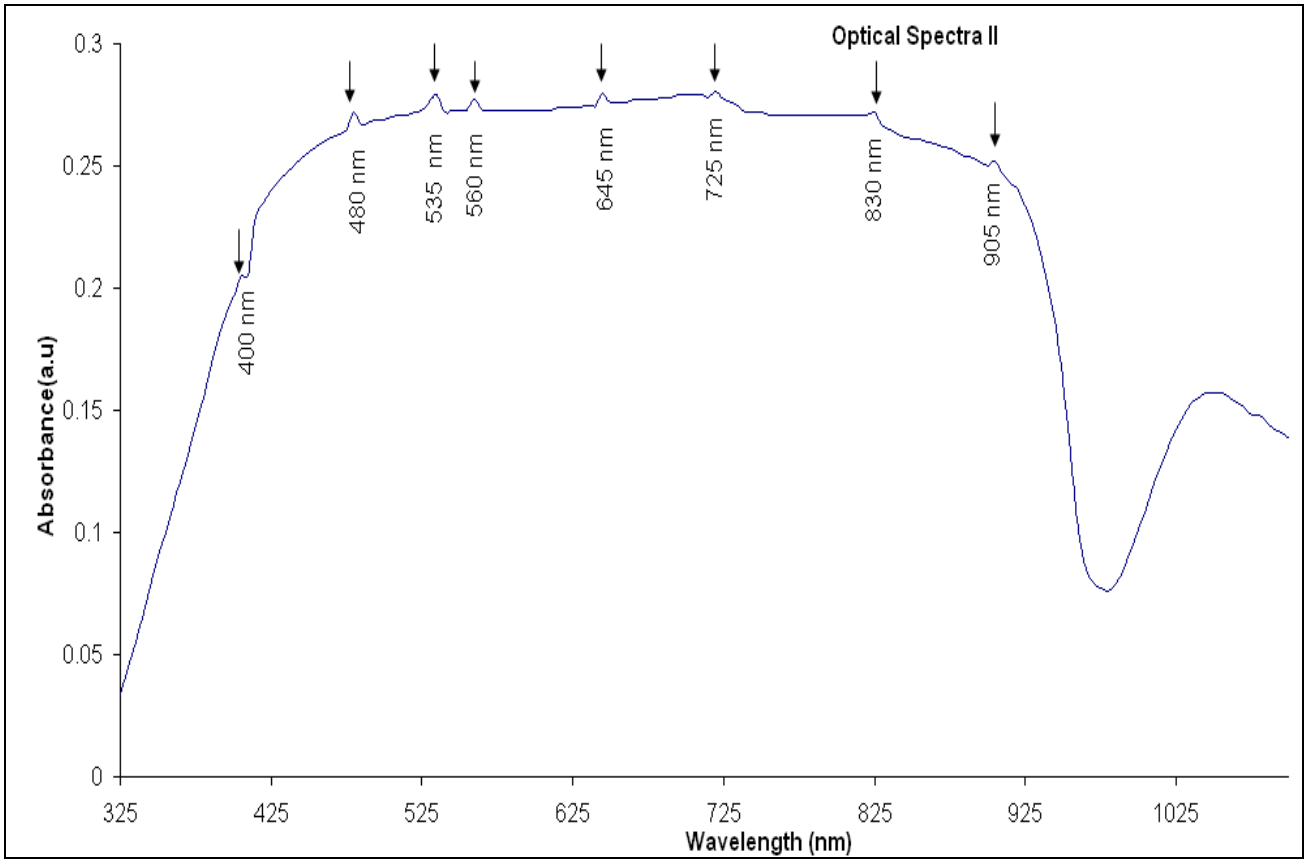
Optical Spectra II
Absorbance(a.u)
Wavelength (nm)
0.3
0.25
0.2
0.15
0.1
0.05
0
325
425
525
625
725
825
925
1025
400 nm
480 nm
535 nm
560 nm
645 nm
725 nm
830 nm
905 nm

Fig. 4(b)

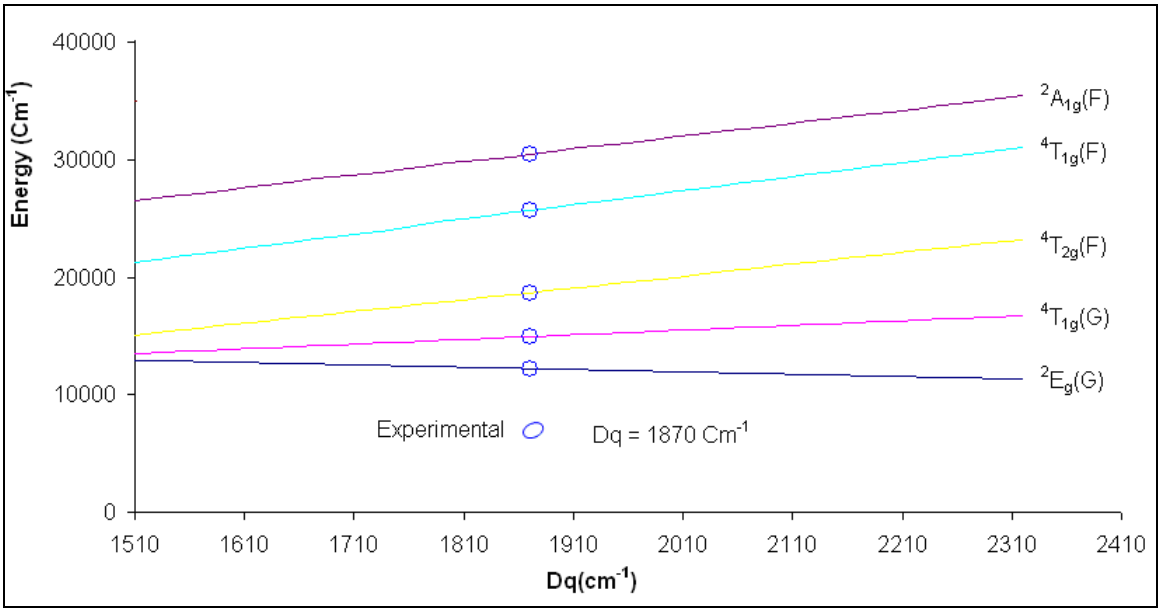
40000
30000
20000
10000
0
Energy (Cm-1)
1510
1610
1710
1810
1910
2010
2110
2210
2310
2410
Dq(cm-1)
2A1g(F)
4T1g(F)
4T2g(F)
4T1g(G)
2Eg(G)
Experimental
Dq = 1870 Cm-1

Fig. 5